BOILING INDUCED MIXED CONVECTION IN COOLING LOOPS

J.U. KNEBEL, G. JANSSENS-MAENHOUT, U. MÜLLER
Institut für Angewandte Thermo-und Fluiddynamik,
Forschungszentrum Karlsruhe — Technik und Umwelt,
Karlsruhe, Germany

ABSTRACT

This article describes the SUCO program performed at the Forschungszentrum Karlsruhe. The SUCO program is a three-step series of scaled model experiments investigating the possibility of a sump cooling concept for future light water reactors. In case of a core melt accident, the sump cooling concept realises a decay heat removal system that is based on passive safety features within the containment. The article gives, first, results of the experiments in the 1:20 linearly scaled SUCOS-2D test facility. The experimental results are scaled-up to the conditions in the prototype, allowing a statement with regard to the feasibility of the sump cooling concept. Second, the real height SUCOT test facility with a volume and power scale of 1:356 that is aimed at investigating the mixed single-phase and two-phase natural circulation flow in the reactor sump, together with first measurement results, are discussed. Finally, a numerical approach to model the subcooled nucleate boiling phenomena in the test facility SUCOT is presented. Physical models describing interfacial mass, momentum and heat transfer are developed and implemented in the commercial software package CFX4.1. The models are validated for an isothermal air-water bubbly flow experiment and a subcooled boiling experiment in vertical annular water flow.

1. INTRODUCTION

Supposing a core melt down accident and considering the problem of melt stabilization and decay heat removal, these requirements can be achieved by an initially dry spreading of the core melt on the containment basemat in combination with a passive sump water flooding and passive cooling from above. This sump cooling concept is sketched in Knebel and Müller (1997). After the flooding of the core melt, the decay heat is transferred from the core melt to the sump water by evaporation, convection and conduction. Condensers are provided to recondense the evaporating sump water. In addition, a natural sump water circulation transports the decay heat to water cooled heat exchangers. Considering the decrease of the decay heat with time, two characteristic mechanisms of decay heat removal can be distinguished: the short-term behaviour that is characterized by mixed single-phase and two-phase natural circulation phenomena due to the high local heat fluxes along the core melt surface, and the long-term behaviour that shows single-phase natural circulation phenomena.
At the Forschungszentrum Karlsruhe the feasibility of the sump cooling concept is investigated by the SUCO program that consists of scaled model experiments and numerical calculations, table 1. Here, the experiments in the SUCOS-2D test facility and first measurement results from the SUCOT test facility are discussed.
The objectives of the SUCOS test facilities are integral phenomenological thermo- and fluiddynamic investigations for the long-term single-phase behaviour. The dominating fluiddynamic process, the pool mixing, is scaled correctly as the Richardson number ratio is equal to unity, Knebel and Müller (1997).

Table 1: SUCO program at the Forschungszentrum Karlsruhe.

Parameters	Future LWR 1300 MW Scale 1:1	SUCOT Volume 1:356 Power 1:356 Heights 1:1	SUCOS-3D Lengths 1:20 Power 1:20^3 Heights 1:20	SUCOS-2D Lengths 1:20 Power 1:20^3/4 Heights 1:20
Working fluid	*water*	*water*	*water*	*water*
Spreading area, m^2	*160*	*0.45*	*0.4*	*0.4/4*
Water height, m	*5.5*	*5.5*	*0.275*	*0.275*
Initial decay heat, MW	*25*	*0.07*	*0.003125*	*0.003125/4*
Initial heat flux, W/cm^2	*15.6*	*15.6*	*0.783*	*0.783*
Investigated behaviour		*short-term two-phase*	*long-term single-phase*	
Code		*CFX4.1*	*FLUENT*	

Altogether, 140 different parameter variations are investigated, the parameters are heating power, distribution of heating power, heat exchanger configuration, heat exchanger inlet temperature, flow resistances, sump water height, three-dimensional effects. The nomenclature of the heat exchangers is given in fig. 1, being a sketch of the SUCOS-2D test facility. The experiments are performed as steady-state and transient experiments according to the heating power.
The objectives of the SUCOT test facility are two-phase natural circulation flow phenomenology such as a) subcooled and saturated pool boiling and flow boiling, b) flow pattern and flow instabilities, c) formation, rise and collapse of steam bubbles and d) influence of heated plate surface structure on boiling.

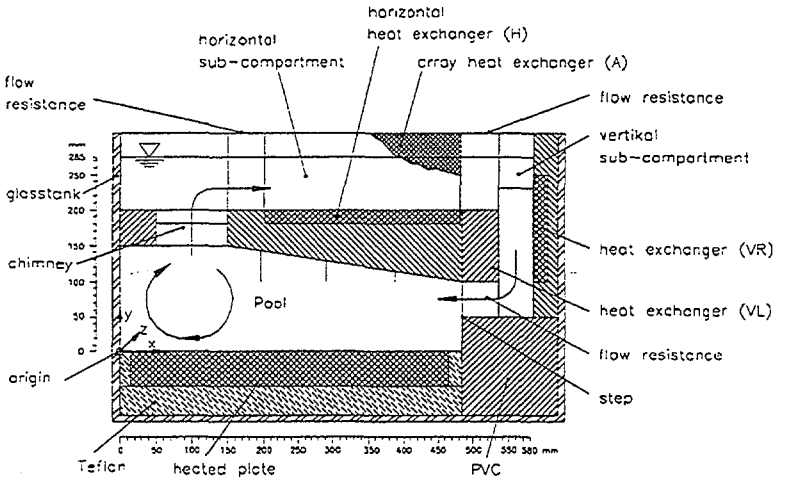

FIG. 1. Sketch of the SUCOS-2D test facility.

2. TEST FACILITY SUCOS-2D

Generally, a stable clockwise natural circulation flow is observed for all heat exchanger configurations investigated. Above the heated plate a well-defined mixing zone with high horizontal velocities establishes. The pool above is isothermal and stagnant and acts as an intermediate and homogeneous heat storage. Below the chimney a large eddy is observed. Along the heat exchangers thin boundary layers are found. The pool temperature is proportional to the heat exchanger inlet temperature. A non-uniform distribution of the heating power does not influence the mean pool temperature in the 2D case, however, in the three-dimensional test facility changes in the thermal stratification in the sump area are observed. Increasing flow resistances lead to increasing pool temperatures due to a decrease in natural circulation.

Steady-State Experiments

The optimisation of the heat exchanger arrangement in the small-scale test facilities SUCOS is done with respect to minimising both the surface area of the heat exchangers and the mean pool temperature. The results are given in table 2. The heating power is *40%* of the initial decay heat. The surface area of the heat exchangers A_{HX} and the mean pool temperature ΔT_{Pool} are normalised by the values of the original arrangement H+VR from Weisshäupl and Bittermann (1993). The pool temperature is taken relative to the heat exchanger inlet temperature. The stable stratification above the horizontal heat exchanger H results in a very inefficient heat transfer characteristic. A replacement of the horizontal heat exchanger by a second vertical heat exchanger VL and two array heat exchangers 2A results in a value of *0.66* for the normalised pool temperature that is considerably lower than the one in the original arrangement. At the same time, the heat transfer area and thus the technical equipment used can be kept the same. The array heat exchangers are installed along both sides of vertical concrete walls of one meter thickness in order to prevent them from damage due to shock waves. As a result, the optimum heat exchanger arrangement is VR+VL+2A.

Table 2: Surface area of the heat exchangers and pool temperature of test facility SUCOS for different heat exchanger arrangements. The heating power is *40%* of the initial decay heat. Reference arrangement is H+VR from Weisshäupl & Bittermann (1993).

Heat exchanger arrangement	chimney blockage	$A_{HX} / A_{HX,Ref}$	$\Delta T_{Pool} / \Delta T_{Ref}$	heat exchanger arrangement	chimney blockage	$A_{HX} / A_{HX,Ref}$	$\Delta T_{Pool} / \Delta T_{Ref}$
H	*0%*	*0.66*	*1.66*	VR+VL	*67%*	*0.56*	*1.02*
VR	*0%*	*0.35*	*1.38*	H+VR+VL	*67%*	*1.22*	*0.82*
H+VR	*0%*	*1.00*	*0.94*	2A	*67%*	*0.44*	*1.09*
VR+VL	*0%*	*0.56*	*0.99*	H+2A	*67%*	*0.94*	*0.85*
H+VR+VL	*0%*	*1.22*	*0.77*	VR+VL+2A	*67%*	*1.00*	*0.66*
H+VR+VL+4A	*0%*	*1.94*	*0.51*	H+VR+2A	*67%*	*1.29*	*0.63*
H	*67%*	*0.66*	*1.82*	H+VR+VL+2A	*67%*	*1.50*	*0.56*
VR	*67%*	*0.35*	*1.40*	H+VR+VL+4A	*67%*	*1.94*	*0.53*
H+VR (Ref.)	*67%*	*1.00*	*1.00*	VR+VL	*200 mm*	*0.44*	*1.27*

Transient Experiments

Figure 2 gives typical results of transient experiments in the SUCOS-2D test facility for three characteristic heat exchanger configurations, the pool temperature T_{Pool} and the heating power Q being plotted versus the scaled time t. The index M denotes model findings. The pool temperature is taken relative to the heat exchanger inlet temperature T_{HX}. Both the heating power and the pool temperature are normalized by the initial values at $t = 0$ for steady-state conditions.
The heating power is reduced according to $Q \propto t^{-1.0}$. Using the local one-dimensional balance equations along the natural circulation loop one can derive a proportionality between the pool temperature and the heating power of $T_{Pool} \propto Q^{1/3}$. Thus, the pool temperature decay can be described by $T_{Pool} \propto t^{-0.33}$. The pool temperature decay curves in fig. 2 fall perfectly together in one curve showing self-similar behaviour. The experiments give an exponent of -0.18, thus reproducing the physics of the relationship from above well.

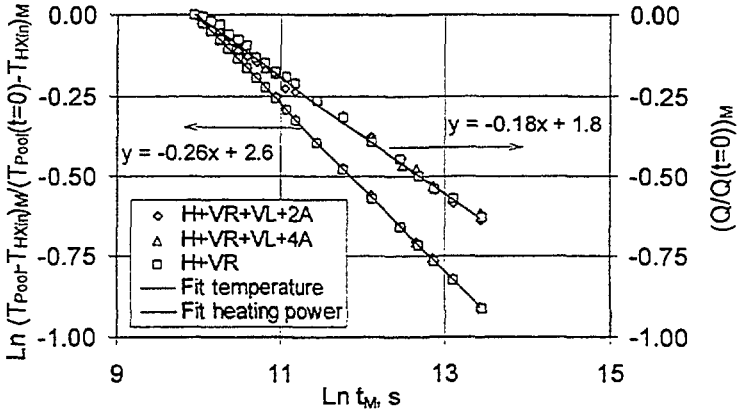

FIG. 2. Pool temperature and heating power bersus time fot the SUCOS-2D test facility. Nomenclature see fig. 1.

In order to scale-up the model findings (index *M*) to prototypic conditions (index *P*), the integral heat transfer characteristics of the natural circulation system has to be known. For the scaled SUCOS-2D test facility, the integral heat transfer characteristic can be described by a laminar heat transfer correlation of the form $Nu \propto Gr^{1/4}$, see Knebel and Müller (1997). The Rayleigh number for the model is in the order of $Ra = 5 \cdot 10^9$. As for the prototype a Rayleigh number in the order of $Ra = 2 \cdot 10^{14}$ is expected, a turbulent heat transfer correlation of the form $Nu \propto Gr^{1/3}$ is chosen.
Considering the transient experiments of figure 2 with a secondary side temperature of $20°C$, one can scale-up to the prototype pool temperatures in the long-term behaviour given in figure 3. A well subcooled pool is found for the heat exchanger configurations that operate two or four of the array heat exchangers (H+VR+VL+2A and H+VR+VL+4A). The temperatures above saturation temperature for heat exchanger configuration H+VR indicate pool boiling conditions. The pool temperature in the prototype is calculated by

$$T_{Pool\,P} = T_{HX,in\,P} + 2.7\left(T_{Pool} - T_{HX,in}\right)_M + \left(c_T - 2.7\right)\left(a \cdot T_{HX,in} + b\right)_M \quad . \tag{1}$$

The coefficient c_T is a characteristic value for the heat exchanger configuration, a and b are geometric parameters, equ. (1) being corrected in comparison to a misprint in Knebel and Müller (1997). The transformation of the velocity is done according to

$$u_P = 7.37\, u_M \quad , \tag{2}$$

which results in maximum values of *0.2 m/s* in the prototype.

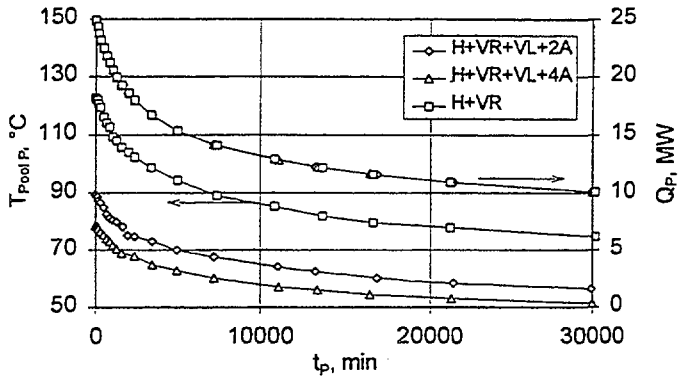

FIG. 3. Pool temperature and decay heat versus time for a prototype geometry.

3. TEST FACILITY SUCOT

The SUCOT test facility is a real height model experiment with a power and volume scale of 1:356, see fig. 4. The local heat flux ratio is kept equal to unity. The heated bottom plate is divided into seven section which can be controlled individually. The front and the back wall of the test facility are made of large glass windows allowing for flow visualization (shadow graph, laser light sheet). Various flanges are provided to introduce traversable instrumentation, such as thermocouple rakes for temperature and twin-fiber optic probes for void measurement. In addition, the void is measured using a gamma-densitometer (Caesium 137). A Laser Doppler anemometer LDA for the measurement of the liquid velocity in the single-phase regions is provided, the bubble velocity will be measured using particle image velocimetry PIV. The system pressure is limited to ambient conditions.

Using the same working fluid as in a real reactor, this test facility preserves the phase change number N_{PCh} and the subcooling number N_{Sub} correctly. The phase change number has recently been renamed as Zuber number N_{Zu} in recognition of Zuber's most significant contributions to the field. The phase change number and the subcooling number are the control parameters of the test facility.

Phase change or Zuber number:

$$N_{PCh} = N_{Zu} = \frac{\Delta h}{\Delta h_{LG}} \frac{\Delta \rho}{\rho_G} = \frac{\dot{Q}/\dot{m}}{\Delta h_{LG}} \frac{\Delta \rho}{\rho_G} = \frac{mass\ flux\ due\ phase\ change}{inlet\ mass\ flux} \quad , \tag{3}$$

Subcooling number:

$$N_{Sub} = \frac{\Delta h_{sub}}{\Delta h_{LG}} \cdot \frac{\Delta \rho}{\rho_G} = \frac{subcooling}{latent\ heat} \quad . \tag{4}$$

The phase change number N_{PCh} takes into account the change of phase due to heat transfer to the sump water. The subcooling number N_{Sub} scales the subcooling of the sump water entering the heated section and, thus, the dimension of the purely liquid region along the core melt. These two numbers are important for the scaling of both the dynamic and the steady-state conditions of a natural circulation system.

In fig. 5 characteristic temperature profiles above the heated plate are given. The subcooled fluid heates up in a thin mixing layer, the pool above being isothermal. The thickness of the boundary layer increases with decreasing x. This is in perfect agreement with the findings in the small-scale test facilities SUCOS, see Knebel and Müller (1997). At $x = 1400\ mm$ the fluid in the mixing layer has reached a value that is above pool temperature, however, still being single-phase flow.

In the chimney, at an elevation of $y > 3\ m$, the fluid reaches saturation conditions due to geodesic pressure relief. Vapour bubbles are generated. The flow regime is bubbly flow. At a frequency of *1/60 Hz* the phenomenon of geysering is observed, which results in a violent vapour production. During geysering, the fluid surface is elevated by about *0.5 m*. The flow regime is observed to be churn turbulent.

The next set of experiments will aim at reaching saturation conditions and a net vapour production at the downstream end of the heated plate.

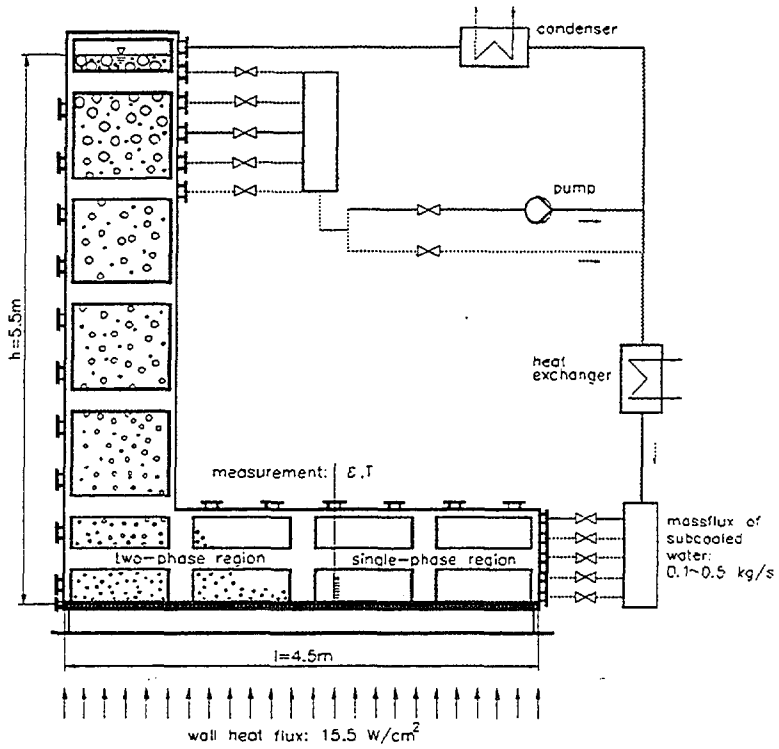

FIG. 4. Sketch of the SUCOT test facility at the Forschungszentrum Karlsruhe.

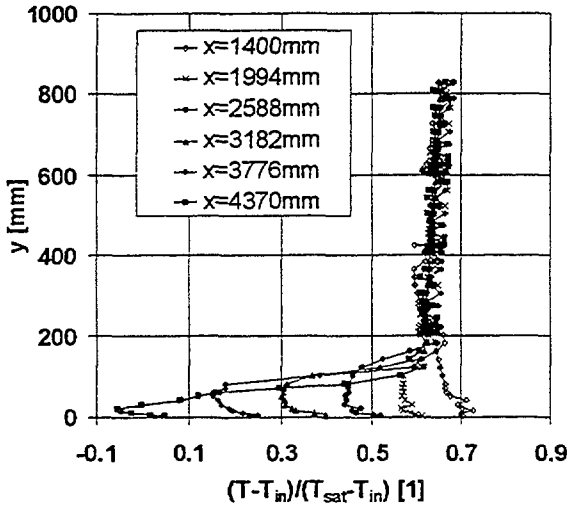

FIG. 5. Temperature profiles above the heated plate for the SUCOT test facility.

First local void measurements are made using a fibre-optic probe. The probe has an outer diameter of *0.6 mm*, the tip being of conical shape with an internal angle of 90°. The surface is polished. The fibre is loaded with *850 nm* light of an LED. The probe is used as a phase identifier: The light is not reflected or reflected from the tip depending on whether the probe is in contact with the liquid phase or the gas phase. The reflected light is detected by a photo-diode. Figure 6a gives the typical signal of a fibre-optic probe, the signal being from bubbles of about *5 mm* diameter that are ejected through a nozzle in stagnant water at a volume flux of *8 l/h*. The sampling frequency is *10 kHz*. The signal shows a very sharp rise both as the bubble hits the probe and as the probe is re-wetted again. Thus, the threshold above which the signal is considered a bubble is a level just above the noise level. A typical threshold is *10%* of the difference between the gas phase level and the liquid phase level. Plotting the cumulative probability density function, fig. 6b, the local void of the above signal is found to be *12%*, the threshold being *10%*.

The next step will be the utilisation of a twin fibre-optic probe to measure the interfacial velocity, the interfacial area concentration and the mean Sauter diameter, as described in Hibiki, Hogsett and Ishii (1997).

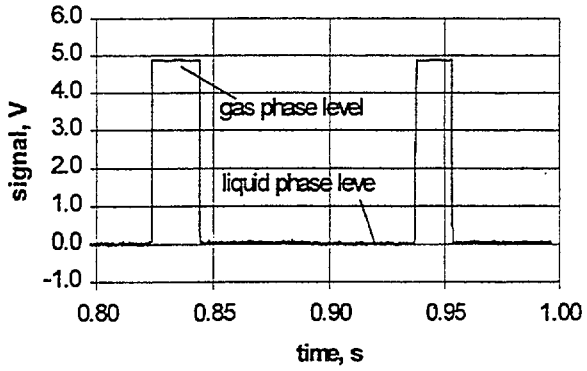

FIG. 6a. Typical signal of fibre-optic probe (recording window of 0.2 s).

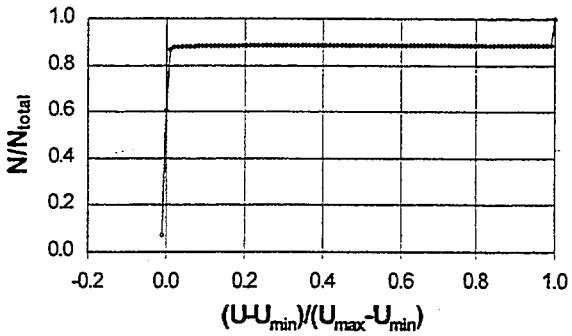

FIG. 6b. Cummulative probability density function.

4. PHYSICAL MODEL DESCRIPTION

The model of interfacial mass, momentum and heat transfer originates with the two-fluid model for disperse flow. Both phases the continuous water and the disperse vapour phase are described by the ensemble-averaged mass, momentum and energy transport equations.

Mass conservation equation:

$$\frac{\partial\left(\varepsilon_k \rho_k\right)}{\partial t}+\nabla\cdot\left(\varepsilon_k \rho_k \left\langle \vec{u}_k \right\rangle_k\right)= \underbrace{\left\langle \Gamma_k \right\rangle_k}_{Vapour-Source} \tag{5}$$

Momentum conservation equation:

$$\frac{\partial\left(\varepsilon_k \rho_k \left\langle \vec{u}_k \right\rangle_k\right)}{\partial t}+\nabla\cdot\left(\varepsilon_k \rho_k \left\langle \vec{u}_k \right\rangle_k \left\langle \vec{u}_k \right\rangle_k\right)$$

$$= -\nabla\left(\varepsilon_k p_k\right)+\varepsilon_k \rho_k \vec{g}+\nabla\cdot\varepsilon_k\left(\left\langle \overline{\overline{\tau}}_k \right\rangle_k+\left\langle \overline{\overline{\tau_k^{Re}}} \right\rangle_k\right)+ \underbrace{\left\langle \vec{I}_k \right\rangle_k}_{Interfacial\ Forces} +\left\langle \vec{f}''_k \right\rangle_k \tag{6}$$

Energy conservation equation:

$$\frac{\partial\left(\varepsilon_k \rho_k \left\langle h_k \right\rangle_k\right)}{\partial t}+\nabla\cdot\left(\varepsilon_k \rho_k \left\langle \vec{u}_k \right\rangle_k \left\langle h_k \right\rangle_k\right)$$

$$= \varepsilon_k \lambda_k \Delta\left\langle T_k \right\rangle_k + \underbrace{\nabla\cdot\left\langle \vec{q}''_{ik} \right\rangle_k}_{Interfacial\ Heat\ Flux} +\left\langle h''_{ik} \right\rangle_k \tag{7}$$

The modelling of the interphase transport phenomena is done for dilute bubbly flow, with air bubbles as small spherical particles. The momentum exchange is described in equ. (2) by a summation of the interfacial forces $\left\langle \vec{I}_k \right\rangle_k$. This results in equ. (4) from an averaging of the forces on a particle volume, induced by the surrounding fluid, derived under Lagrangian approach.

$$\langle \underline{I}_L \rangle_L = \underbrace{-C_D \frac{3\varepsilon_G}{4D_B}\rho_L \left|\langle \underline{u}_G \rangle_G - \langle \underline{u}_L \rangle_L\right| \left(\langle \underline{u}_G \rangle_G - \langle \underline{u}_L \rangle_L\right)}_{\text{Drag Force}} - \underbrace{C_{TD}\rho_L k_L \nabla \varepsilon_G}_{\text{Turbulent Diffusion}}$$
$$\underbrace{-C_L \rho_L \varepsilon_G \left(\langle \underline{u}_G \rangle_G - \langle \underline{u}_L \rangle_L\right) \times \left(\nabla \times \underline{u}_L\right)_L}_{\text{Lift Force}} \underbrace{- C_{VM}\rho_L \varepsilon_G \left(\left\langle \frac{D\underline{u}_G}{Dt} \right\rangle_G - \left\langle \frac{D\underline{u}_L}{Dt} \right\rangle_L\right)}_{\text{Virtual Mass}} \qquad (8)$$

The first term in equ. (4) represents the drag force. This friction force is modelled with the projected interfacial flow area and the drag coefficient C_D, which is in the turbulent Newton regime $C_D = 0.44$. The second term is the turbulent diffusion force, which represents the local changes in dynamic pressure at the interface. This term is modelled with the turbulent kinetic energy and with a turbulent diffusion coefficient $C_{TD} = 0.1$ for a disperse bubbly flow. The third term is the lift force, acting on bubbles which are unequally surrounded by the fluid flow. The lift term is modelled with a lift coefficient $C_L = 0.5$ for weakly viscous flows. The last term represents the virtual mass, which is implemented for steady state flows and is modelled with a virtual mass coefficient $C_{VM} = 0.5$ as analytically derived for an isolated bubble.

The modelling of the vapour source is done for subcooled nucleate boiling under low pressure with models valid only for water as fluid and for moderate wall heat fluxes. The vapour generation model is based on bubble formation and detachment mechanisms, the condensation model on bubble growth and shrinking mechanisms. The vapour inside the bubble and the bubble surface are assumed to remain at saturation temperature, modelled as a function of the pressure in the bubble. The vapour generation rate Γ_G at the wall is determined under a mechanistic approach as a function of the bubble release frequency f which depends on the given wall heat flux q''_W, of the bubble departure diameter D_D, and of the active nucleation site density N, which depends on the calculated wall temperature T_W.

$$\Gamma_G = \frac{\pi D_D^3}{6}\rho_G \cdot \underbrace{f(q''_W)}_{\text{Detachment frequency}} \cdot \underbrace{N(T_W)}_{\text{Nucleation site density}} \qquad (9)$$

The mechanism of bubble formation is described with the active nucleation site density N given by an empirical correlation of Dhir and Wang (1993),

$$N = 5.8\ 10^{-23.4} \cdot \frac{1-\cos\phi}{D_C^{5.4}}\ , \qquad (10)$$

as a function of the surface wetting angle ϕ and of the critical bubble diameter D_C, which is approximately inversely proportional to the wall superheat

$$D_C = \frac{4\sigma T_{Sat}}{\rho_G\, \Delta h_{LG}\,(T_W - T_{Sat})}\ . \qquad (11)$$

The mechanism of bubble detachment is described with the detachment frequency f and the bubble detachment diameter D_D. The major parameter in literature characterising heat transfer in boiling is the product $f \cdot D_D^a$. D_D^a with the power $a = 1$ for the system water/vapour under atmospheric conditions. This product $f \cdot D_D$ is given as "bubble departure velocity", depending on the wall heat flux q''_W by a correlation of Malenkov (1973).

$$f \cdot D_D = \frac{u_B}{\pi}\left(1 - \frac{1}{1 + u_B \Delta h_{LG}\rho_G / q''_W}\right)^{-1} \ ;\ u_B = \left(\frac{D_D g \Delta\rho}{2(\rho_G + \rho_L)} + \frac{2\sigma}{D_D(\rho_G + \rho_L)}\right)^{1/2} \qquad (12)$$

The bubble departure diameter D_D is expressed by a correlation of Cole and Rohsenow, see Dhir (1990) using a dimensionless Laplace length and a Jakob number Ja.

$$D_D = 1.5\ 10^{-4}\left(\frac{\sigma}{g\Delta\rho}\right)^{1/2} Ja^{5/4} \ ;\ Ja = \frac{\rho_L\, c_{pL}\, \Delta T_{Sat}}{\Delta h_{LG}\, \rho_G} \qquad (13)$$

In the condensation model no coalescence or fragmentation is assumed for the dilute bubbly flow in the subcooled region. The bubble size variations are coupled to changes in void fraction. During condensation the bubble diameter change rate obeys the following energy balance

$$\Delta h_{LG} \frac{d}{dt}\left(\rho_G \frac{\pi}{6} D_B^3\right) = \alpha_{BI}\,(T_{Sat} - T_L)\,\pi D_B^2\ . \qquad (14)$$

The heat transfer coefficient α_{BI} in equ. (10) is defined by the Nusselt number Nu, given by a correlation of Ranz and Marshall (1952).

$$Nu_B = 2 + 0.6\ Re_B^{0.5}\ Pr_L^{0.3} \quad with \quad Nu_B = \frac{\alpha_{BI} D_{BI}}{\lambda_L} \qquad (15)$$

Solving equ. (10) yields the typical relation between the bubble diameter D_B and the time $t^{2/3}$, which is in agreement with literature on bubble growth.

5. VALIDATION OF THE PHYSICAL MODELS

Isothermal Air-Water Bubbly Flow Experiment

At the Forschungszentrum Karlsruhe an isothermal air-water bubbly flow experiment has been performed by Samstag (1996). In a vertical pipe of *5000 mm* length and internal diameter D = *70.34 mm* the axial development and the radial redistribution of air bubbles have been measured for symmetric and non-symmetric air injection types. The water was injected at the entrance section with a superficial fluid velocity of J_L = *1.08 m/s*. The water flow is turbulent, the Reynolds number being in the range of $0.25E5 < Re_L < 1.E5$. Air with a superficial velocity of J_G = *0.12 m/s* could be injected through the central nozzle and *6* surrounding concentric nozzles. The bubbles generated by the nozzles could be characterised as spherical particles with a diameter mainly varying from *2 mm* to *4 mm*. Four different types of air injection have been analysed: through all nozzles, through the central nozzle, through *1* eccentric nozzle and through *2* opposite nozzles. The spatial bubble distribution is measured in distinct horizontal sections by Röntgen-Tomography, hot wire probes and resistance probes.
The simulation of the flow using CFX4.1 is done within a three-dimensional geometry. Starting from the measured profiles for the void, the velocity and the turbulent kinetic energy at the entrance section at *5D (= 35 mm)* height, the profiles at the section at *10D (= 700 mm)* height and *63D (= 4430 mm)* height have been calculated for the *4* different types of air injection. The bubbles are simulated as small spherical particles with a mean diameter D_B = *3 mm*. Different classes of bubble sizes were not simulated, as the present models are not sensitive to bubble size and bubble interactions.
Figures 7a and 7b show the measured and calculated void profiles across the tube diameter at *10D (= 700 mm)* height and at *63D (= 4430 mm)* height respectively, for the symmetric case of air injection through all nozzles. The formation of a lubricated ring profile for the void and the azimuthal redistribution of the bubbles around the wall, mainly caused by the lift force in the non-developed flow region remain recognisable for all heights investigated. The calculations, with the additional models for the interfacial forces included, reproduce the void profile well. Without these additional models, the calculation shows a void profile with decreased peaks around the wall and the creation of a high void in the centre of the tube. Thus, a calculation without the additional models is not applicable for this non-developed bubbly flow.
Similar results for the other symmetric case with air injection through the central nozzle are given in Figs. 8a and 8b. In the subsequent presentation of the simulation results, the calculations without additional models have been omitted as no additional information can be gained. For the non-symmetric case of air injection through one eccentric nozzle the Figs. 9a and 9b show the measured and calculated void profiles across the middle of the open eccentric nozzle. Here a turbulent bubble transport along the wall can be observed by the decrease of bubble concentration above the eccentric nozzle and by the build-up of a bubble concentration along the wall. In this case the turbulent diffusion causes mainly the dispersion of the bubbles in the radial void profiles. For the case of air injection through two opposite nozzles, Figs. 10a and 10b, the void profiles are almost the same as in Figs. 7a and 7b, as they are again affected by the lift force and the turbulent diffusion force.
In general, the experimental and the numerical results are in good agreement and show a bubble transport towards the wall for the axial positions measured. This emphasises the importance of the lift force, partially counteracted by the turbulent diffusion force. Comparing different cases of air injection with the same global void fraction of *0.10*, a difference in void profile at *63* diameters height was still present, varying from double peaked, as expected for a non-developed two-phase flow to single peaked, as expected for a developed two-phase flow. This shows that the length of flow establishment for turbulent multi-phase flows is significantly longer than for turbulent single-phase flows.

Subcooled Boiling Experiment In Vertical Annular Water Flow

The implemented boiling model is validated against the experiment of Bibeau and Salcudean (1994), investigating subcooled boiling in vertical annular water flow. Along the symmetry axes of a vertical pipe of *600 mm* length and with internal diameter D = *17.0 mm*, an internal heater of *9 mm* diameter is placed, acting as a variable heat source. Water is injected at the entrance section with a superficial fluid velocity of J_L = *0.134 m/s*, performing a laminar annular water flow. The inlet temperature of the subcooled water could be varied as $T_{L,in}$ = *45°C*, $T_{L,in}$ = *60°C and* $T_{L,in}$ = *75°C* and the pressure at the outlet section at *35D (= 600 mm)* could be varied as p = *1 bar*, p = *2 bar* and p = *3 bar*. The heat source Q is varied between *0 kW* and *60 kW*, generating vapour bubbles along the heater surface after the point of onset of nucleate boiling. At

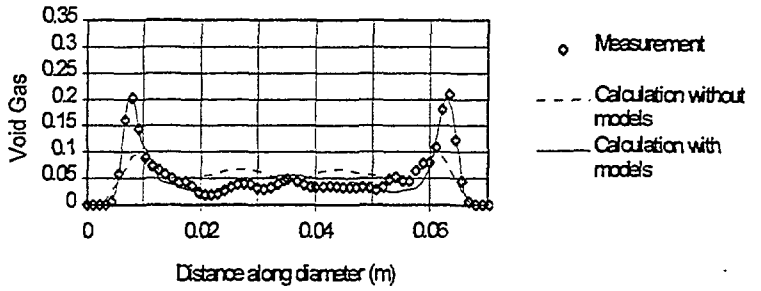

Void profile at *10 D* height

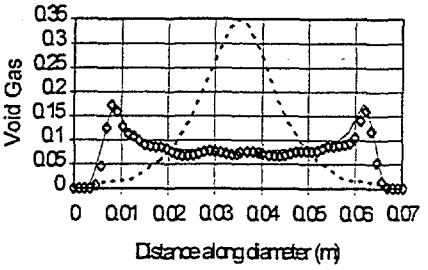

Void profile at *63 D* height

FIG. 7. Air injection through all nozzles.

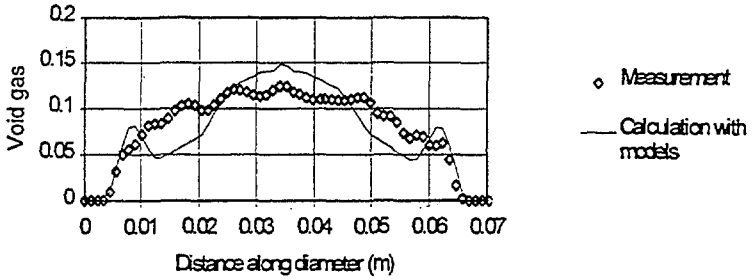

Void profile at *10 D* height

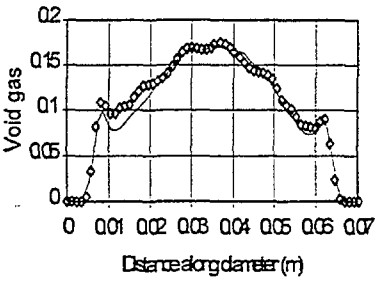

Void profile at *63 D* height

FIG. 8. Air injection through the central nozzle.

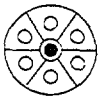

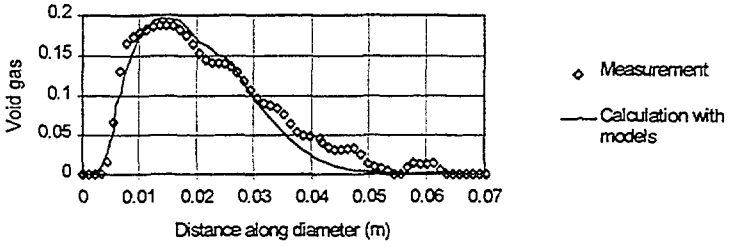

Void profile through the middle of the nozzle at *10D* height

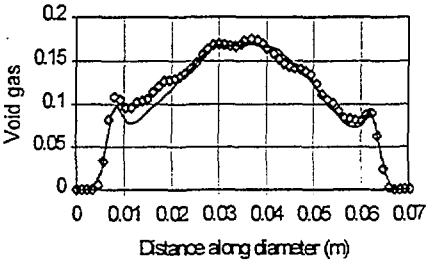

Void profile through the middle of the nozzle at *63D* height

FIG. 9. Air injection through one eccentric nozzle.

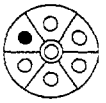

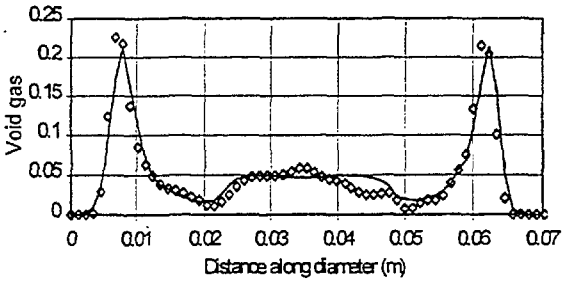

Void profile through the middle of two nozzles at *10D* height

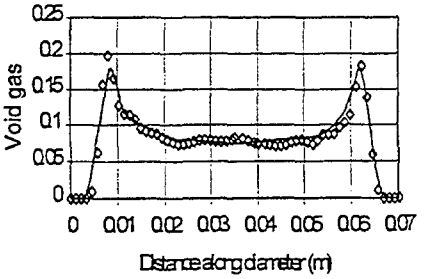

Void profile through the middle of two nozzles at *63D* height

FIG. 10. Air injection through two opposite nozzles.

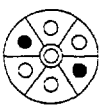

the measurement section at *32D (= 550 mm)* height the vapour volume fraction has been measured by Gamma-Densitometry for different heat sources. For steady state conditions with a given liquid flow rate each measured volume fraction thus corresponds to one imposed heat flux.
The geometry is simulated in two dimensions. The vapour generation source is additionally implemented in CFX4.1 using the models from before. Each measurement point is simulated separately. As the wall temperature is the important parameter in the vapour generation model, the temperature profile along the wall has to be calculated using a time-marching method. When steady-state conditions are reached the vapour generated at the measurement section could be integrated over the cross-section.
In Fig. 11 the integral void generated and the wall temperature achieved at the measurement section are presented versus the equilibrium quality of the mixture x_{eq}, for the case of an inlet temperature of $T_{L,in} = 60°C$ and an outlet pressure of $p = 2\ bar$. The equilibrium quality x_{eq} is defined as the ratio of the enthalpy consumed by the mixture to evaporate to the latent heat.

$$x_{eq} = \frac{\Delta h_L - \Delta h_{Sub}}{\Delta h_{LG}} = \frac{\dot{Q}/\dot{M} - c_{pL}\left(T_{Sat} - T_{L,in}\right)}{\Delta h_{LG}} \tag{16}$$

Six cases of imposed heat source Q, corresponding to $x_{eq} = -11.6\%, -10.5\%, -10.1\%, -7.9\%, -5.5\%$ and -4.0%, have been chosen to cover the single phase flow regime, to reach the onset of nucleate boiling and to finally cover the fully established nucleate boiling regime. Each of them are calculated with the extended two-fluid-model. Both the onset of nucleate boiling and the total void are in good agreement with the experimental data, the experimental error bashing given in the diagram. The corresponding increasing wall temperatures are also shown. As long as no void is generated the calculated wall temperature increases with a slope as found in single-phase calculations. The difference in the calculated and experimental wall superheated temperature is within the range of standard deviations in the measured data.
The influence of the outlet pressure p and the water inlet subcooling $T_{sub} = T_{sat} - T_L$ on the void generated at a certain equilibrium quality x_{eq} has also been checked. With increasing pressure, the saturation temperature increases and the enthalpy of the mixture at the inlet is further removed from the saturation point. The onset of nucleate boiling is therefore moved to a lower equilibrium quality. With decreasing water inlet subcooling, the enthalpy of the mixture at the inlet is closer to saturation. The onset of nucleate boiling occurs at higher equilibrium qualities. These physical behaviours are also found in the numerical results, indicating the correct physical behaviour of the vapour generation model.
In general, the vapour generation at the heated wire in the annular flow is in good qualitative agreement with the experimental results for the onset of nucleate boiling as well as for the amount of vapour generated.

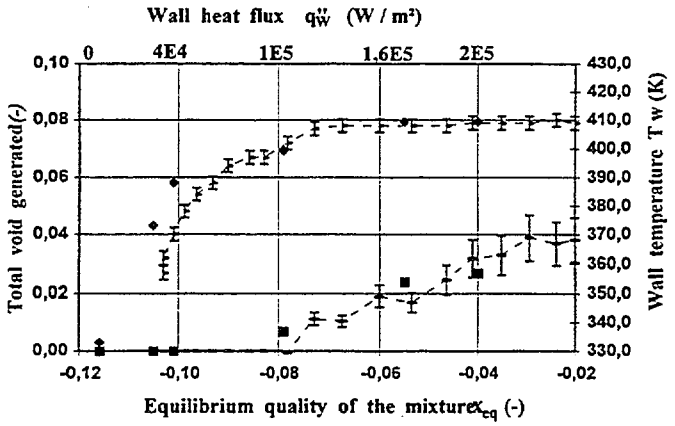

FIG. 11. Void and temperature profile versus the equilibrium quality for subcooled boiling mixture. P=2bar). Void: ■ CFX, — experiment; wall temperature: ◆CFX, — experiment.

SUMMARY

The sump cooling concept for future LWR that realises a passive decay heat removal system in case of a core melt accident, could be significantly improved by substituting the horizontal heat exchanger by several vertical heat exchangers. Providing the same heat transfer area, the pool temperature can be lowered by *44%* relative to the first proposal by Weisshäupl and Bittermann (1993). The temperature decay of the transient experiments in SUCOS-2D shows self-similar behaviour and can be described by $T_{Pool} \propto t^{-0.17}$. A scale-up of

the model pool temperatures to prototypic conditions demonstrates that the long-term decay heat can be removed from the containment having a well subcooled reactor sump. However, subcooled boiling will be observed in the short-term along the core melt surface. The sump cooling concept realizes a long-term decay heat removal system.

The test facility SUCOT is in operation. First experiments show a boundary layer flow above the heated plate and an isothermal pool above. Due to a geodesic pressure relief, violent geysering is observed in the chimney. The fibre-optic probe shows a good performance according to phase identification.

The two-fluid-model of the software package CFX4.1 is extended by physical models to describe interfacial mass, momentum and heat transfer in flows with subcooled nucleate boiling. The models are thoroughly validated against two experiments, an isothermal air-water bubbly flow experiment and a subcooled boiling experiment, which represent good benchmarks to test both the fluiddynamic and the thermodynamic behaviour of the extended two-fluid-model. Now, a validated numerical tool is available to calculate the subcooled nucleate boiling phenomena observed in the test facility SUCOT.

The next step of the present work will be experiments in the SUCOT test facility with net vapour production at the heated plate, and the numerical simulation using CFX4.1.

REFERENCES

Knebel, J.U., Müller, U., Scaling of Passive Decay Heat Removal by Sump Cooling, Jahrestagung Kerntechnk 1997, Aachen, pp. 144-147, 1997.

Bibeau, E.L., Salcudean, M., Subcooled Void Growth Mechanisms and Prediction at Low Pressure and Low Velocity, Int. Journal of Multiphase Flow, 20, pp. 837-863, 1994.

Cole, R., Rohsenow, W., Correlations of Bubble Diameter for Saturated Liquids, Chem. Eng. Prog. 65, pp. 211-213, 1969.

Dhir, V. K., Nucleate and Transition Boiling Heat Transfer under Pool and External Flow Conditions, Proc. 9th Int. Heat Transfer Conf., vol. 1, Jerusalem, Israel, pp. 129-155, 1990.

Dhir, V. K. and Wang, C. H., Effect of Surface Wettability on Active Nucleation Site Density During Pool Boiling of Water on a Vertical Surface, Trans. ASME Journal of Heat Transfer, vol. 115, pp. 659-669, 1993.

Hibiki, T., Hogsett, S., Ishii, M., Local Measurement if Interfacial Area, Interfacial Velocity and Liquid Turbulence in Two-Phase Flow, Proc. OECD/CSNI Spec. Meeting on Advanced Instrumentation and Measurement Techniques, Santa Barbara, USA, March 17-20, 1997.

Malenkov, I. G., Detachment Frequency as a Function of Size for Vapor Bubbles, translated from Inzhenerno-Fizicheskii Zhurnal at the Academy of Sciences of the USSR, vol. 20 , pp. 988-994, 1973.

Ranz, W. E. and Marshall, W. R., Experimental Correlation for Heat Transfer Between Particle and Fluid, Chemical Engineering Prog., vol. 48, pp. 141, 1952.

Samstag, M., Experimental Investigations on Transport Phenomena in Vertical, Turbulent Air-Water Bubbly Flow, Ph.D. Thesis, Mechanical Eng. Dept., Karlsruhe University, 1996.

Weisshäupl, H. A., Bittermann, D., Large Spreading of Core Melt for Melt Retention/Stabilization, Proc. 5th Int. Seminar on Containment of Nuclear Reactors, August 23-24, Karlsruhe, FR Germany, pp. 347-355, 1993.